2023 62nd IEEE Conference on Decision and Control (CDC)
December 13-15, 2023. Marina Bay Sands, Singapore

Trajectory Generation using Activator-Inhibitor Systems

Yazan M. Al-Rawashdeh Mohammad Al Saaideh Almuatazbellah M. Boker Hoda Eldardiry
Marcel F. Heertjes Mohammad Al Janaideh

***Abstract*— It is once said that 'He who wishes to be obeyed must know how to command.' Inspired by this saying, the dynamics of the partially known flexible motion system are considered in the making process of the desired trajectory signals it has to follow by exploiting systems and signals relations. Accordingly, the trajectory generator system activates the motion of the driven system whose tracking performance inhibits the generator and forces it to modify its trajectories while ensuring the desired motion requirements are met. Using singular perturbation theory, a near optimal trajectory generator system is designed, and with the aid of a suitable state observer a cascaded head-to-tail activator-inhibitor system configuration is realized. Essentially, the closed-loop error is fed-back to the trajectory generation process rather than using a limited feedforward controller alone based on the partially known dynamics. The superiority of the proposed technique is compared to the Sine-Squared motion trajectory, and its performance is evaluated through simulation.**

I. Introduction

Typically, precision motion systems follow desired trajectories that are designed offline to fulfill their assigned tasks [1], [2]. Various techniques can be used to design these trajectories such as polynomials [3], and input shapers [4]. In point-to-point positioning, the motion system passes through a sequence of points where the system first accelerates to a prescribed constant velocity during one phase, maintaining that velocity for some time, and then decelerates to reach the (usually zero) terminal velocity. In general, motion systems are flexible [5], [6], which may hinder the attainable precision when their structural modes are excited [7]. When these modes are known, the effect can be foreseen during the design of the desired trajectories [8]–[10], otherwise, they have to be identified first, c.f. [8]. Also, un-modeled disturbances may affect the positioning process severely, and therefore, have to be rejected.

Y. M. Al-Rawashdeh, M. Al Saaideh, and M. Al Janaideh are with the Department of Mechanical and Mechatronics Engineering, Memorial University, St. John's, Newfoundland A1B 3X5, Canada, email: {yalrawashdeh, mialsaaideh, maljanaideh}@mun.ca.

A. M. Boker is with the Bradley Department of Electrical and Computer Engineering, Virginia Tech, Blacksburg, VA, USA, email: boker@vt.edu

H. Eldardiry is with the Department of Computer Science, Virginia Tech, Blacksburg, VA, USA, email: hdardiry@vt.edu.

M. F. Heertjes is with the ASML and Department of Mechanical Engineering at Eindhoven University of Technology, 5612 AZ Eindhoven, Netherlands, marcel.heertjes@asml.com.

M Al Janaideh is also with the School of Engineering, University of Guelph, Guelph, ON N1G 2W1, Canada, and the Department of Mathematics, Czech Technical University, Prague 6, Czech Republic, maljanai@uoguelph.ca.

Inversion-based feedforward controllers are essential in motion systems [11], where the system inverse is used in a feedforward controller handles the predefined and supplied trajectory signals [11], [12]. Desiring a priori nature of the trajectories, c.f. [13], makes them known [14], [15], and therefore, can be shaped [10], or optimized [13] to suit the known dynamics of the motion system, including the known structural modes. In this study, the authors believe that the nature of these trajectories signals is yet to be determined. As for disturbance rejection, feedback controllers are also needed [2] such that acceptable levels of system robustness and disturbance rejection capabilities are obtained.

As stated earlier, in typical point-to-point motion, the motion system undergoes transitions through mainly three phases, i.e., acceleration, constant velocity, and deceleration phases. For time-critical applications like wafer scanners used in the production of computer chips, the first and last phases are considered *non-productive* [14], and therefore, have to be optimized [14]. The constant speed phase is considered the productive phase during which the system-assigned task takes place. Examples of standard motion profiles can be found in [13], where some profiles utilize more than three intervals to include the imposed kinematical constraints.

To optimize the acceleration and deceleration phases, the concept of *minimum energy* can be used with the multi-interval trajectory-making process [16]. In such a process, energy is minimized in any given open sub-interval while the specified motion requirements given in the form of boundary conditions dominate at the ends of that sub-interval. When these intervals have finite time, mainly near-optimal trajectories can be obtained. To that end, a system *singularly perturbed* version of its *known* dynamics must appear in the definition of the trajectory generator system, where the fast subsystems of the singularly perturbed system have longer intervals compared with their dynamics, while their boundary layers appear in the solution of the slow subsystem [16]. This allows the concept of minimum energy to be valid even after the operation time of the driven motion system is optimized. Unfortunately, in many cases, the dynamics of the driven system are only partially known. Consequently, the near-optimal trajectories are not only affected by the interval's time horizons but also by the available information about the system dynamics.

According to the system known dynamics, and as explained in [17], motion requirements in the form of boundary conditions are imposed on an interval within a multi-interval motion trajectory profile. Consequently, the trajectory generator system will generate (near) optimal desired trajectories based on a singularly perturbed version of the motion system dynamics. To improve the results obtained in [17] by specifically addressing the unknown dynamics of the driven motion system and any active disturbances, we propose the activator-inhibitor configuration that is inspired by pattern formation [18] and morphogenesis [19] and is viewed as a cascaded system of the inhibitor, i.e., the motion system, and the activator, i.e., trajectory generator, such that the activator adjusts its trajectories on-line based on the inhibitor status in a way that ensures meeting the desired motion requirements. The performance of [17] is compared to the Sine-Squared motion profile when both benefit from the proposed method under no kinematical constraints. Accordingly, the advantage of trajectory generation using [17] is highlighted, and the possibility of using the herein proposed method independently of [17] is demonstrated.

The problem formulation, driven motion system dynamics, system configurations, and various aspects of the proposed technique are presented in Section II followed by the simulation results and discussion in Section III. Final remarks and future work to extend the applicability of the proposed method are given in Section IV.

II. Problem Formulation

A. Mathematical Model

Consider the motion of a generic flexible and friction-free system (Σ_G) depicted in Fig. 1a- without disturbances ($d = 0$)- given as [5], [6], [17]

$$\Sigma_G := \frac{p_a(s)}{u(s)} = \frac{1}{m_t\, s^2} + \frac{1}{m_t} \sum_{i=2}^{N} \frac{\bar{\alpha}_i}{s^2 + 2\,\bar{\zeta}_i\,\bar{\omega}_i\, s + \bar{\omega}_i^2} \tag{1}$$

where the total mass is denoted by $m_t = \sum_{i=1}^{N} m_i$, with N flexible modes having damping ratios $\bar{\zeta}_i$ and natural frequencies $\bar{\omega}_i$ with $\bar{\alpha}_i$ attainable via modal analysis, and the system input and actual output denoted by u, p_a without disturbances $d = 0$, respectively.

The system Σ_G can be written as [11], [17]

$$\Sigma_G := \begin{cases} \dot{\boldsymbol{x}}_G(t) = \boldsymbol{A}_G\, \boldsymbol{x}_G(t) + \boldsymbol{B}_G\, \boldsymbol{u}(t) \\ p_a(t) = \boldsymbol{C}_G\, \boldsymbol{x}_G(t) \end{cases} \tag{2}$$

where the system dynamical states are $\boldsymbol{x}_G \in \mathbb{R}^{n_G \times 1}$, the system input is $\boldsymbol{u} \in \mathbb{R}^{m \times 1}$, its output is $p_a \in \mathbb{R}$, and the matrices $\boldsymbol{A}_G, \boldsymbol{B}_G$ and $\boldsymbol{C}_G$ are defined with suitable dimensions. According to Fig. 1a, Σ_1 is given as

$$\Sigma_1 := \begin{cases} \dot{\boldsymbol{x}}(t) = \boldsymbol{A}\, \boldsymbol{x}(t) + \boldsymbol{B}\, p_d(t) \\ p_a(t) = \boldsymbol{C}\, \boldsymbol{x}(t) = x_1 \end{cases} \tag{3}$$

where the aggregated state vector $\boldsymbol{x} = \left[\boldsymbol{x}_G^{\mathrm{T}}, \boldsymbol{x}_c^{\mathrm{T}}, \boldsymbol{x}_f^{\mathrm{T}}\right]^{\mathrm{T}} \in \mathbb{R}^{w \times 1}$, with no disturbance, and the corresponding matrices are given as [17]

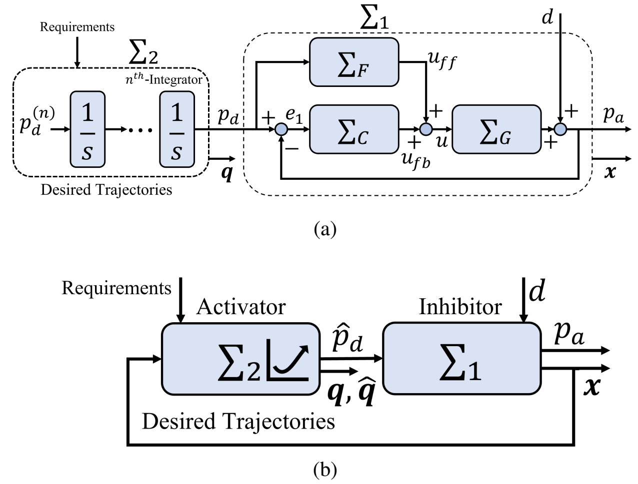

Fig. 1: Block diagram representations of the motion system under feedforward-feedback control scheme with (a) $\Sigma_2 \rightarrow \Sigma_1$ open-loop, and (b) $\Sigma_2 \leftrightarrow \Sigma_1$ head-to-tail closed-loop interactions.

$$\begin{aligned} \boldsymbol{A} &= \begin{bmatrix} \boldsymbol{A}_G - \boldsymbol{B}_G\, \boldsymbol{D}_C\, \boldsymbol{C}_G & \boldsymbol{B}_G\, \boldsymbol{C}_C & \boldsymbol{B}_G\, \boldsymbol{C}_F \\ -\boldsymbol{B}_C\, \boldsymbol{C}_G & \boldsymbol{A}_C & \boldsymbol{0} \\ \boldsymbol{0} & \boldsymbol{0} & \boldsymbol{A}_F \end{bmatrix} \\ \boldsymbol{B} &= \begin{bmatrix} \boldsymbol{B}_G\, (\boldsymbol{D}_C + \boldsymbol{D}_F) \\ \boldsymbol{B}_C \\ \boldsymbol{B}_F \end{bmatrix}, \; \boldsymbol{C} = [\boldsymbol{C}_G, \boldsymbol{0}, \boldsymbol{0}] \end{aligned} \tag{4}$$

and the subsystems given as $\Sigma_G := (\boldsymbol{A}_G, \boldsymbol{B}_G, \boldsymbol{C}_G, \boldsymbol{0})$ with associated states $\boldsymbol{x}_G$, $\Sigma_C := (\boldsymbol{A}_C, \boldsymbol{B}_C, \boldsymbol{C}_C, \boldsymbol{D}_C)$ with associated states $\boldsymbol{x}_c \in \mathbb{R}^{c \times 1}$, and $\Sigma_C := (\boldsymbol{A}_F, \boldsymbol{B}_F, \boldsymbol{C}_F, \boldsymbol{D}_F)$ with associated states $\boldsymbol{x}_f \in \mathbb{R}^{f \times 1}$. We assume that the following assumption holds.

Assumption 2.1: The system Σ_1 under the available controllers is input-to-state stable.

According to Fig. 1a, the *desired* position p_d is produced by the trajectory generator system Σ_2 whose dynamics are given by

$$\begin{aligned} \dot{q}_i &= q_{i+1}, \;\; i = 1, 2, \cdots, l-1 \\ \dot{q}_l &= p_d^{(l)} \end{aligned} \tag{5}$$

with $q_1 \equiv p_d$, and $p_d^{(l)}$ denotes the l^{th} time derivative of p_d that is designed to meet the motion requirements [14]. To ensure smoothness of the desired trajectories, usually $l \geq 3$ is used, i.e., finite jerk values. Note that in Fig. 1a, the $\Sigma_1 \rightarrow \Sigma_2$ interaction occurs under an open-loop configuration, which indicates that Σ_2, i.e., the trajectory generator, is not aware of the status of the driven motion system Σ_1. Specifically, the tracking error $e_1 = p_d - p_a \equiv q_1 - x_1$ does not show up in (5). This motivates us to look into the $\Sigma_1 \leftrightarrow \Sigma_2$ head-to-tail closed-loop interaction depicted in

Fig. 1b.

Remark 2.1: To enhance readability, matrices dimensions are presented when needed, i.e., assumed conformable.

1) Activator-inhibitor cascaded system: To make Σ_2 aware of Σ_1 tracking error e_1, let the dynamics of the tracking error estimate ($\hat{e}$) be given according to the following state estimator (observer)

$$\begin{aligned} \dot{\hat{e}}_i &= \hat{e}_{i+1} + \beta_i\,(x_1 - q_1)\,,\ i = 1, 2, \cdots, n-1 \\ \dot{\hat{e}}_n &= \hat{\sigma} + \beta_n\,(x_1 - q_1) + \beta_0\,(x_{n+1} - q_{n+1}) \\ \dot{\hat{\sigma}} &= \beta_{n+1}\,(x_1 - q_1) \end{aligned} \tag{6}$$

with $n \leq \min(n_G, l)$ to be determined, q_1, q_{n+1} are given by (5), and the constants $\beta_i > 0 \in \mathbb{R}, i = 0, 1, \cdots, n+1$ are chosen such that (6) is stable, where β_0 is chosen to reflect the dependency on the available measurements $x^{(n)} \equiv x_{n+1}$. The choice of n depends on the available measurements (or estimates) of Σ_1; for example when acceleration measurements are available, $1 \leq n \leq 2$ can be used in (6) under which Σ_2 will *activate* Σ_1 using the *modified* desired input ($\hat{p}_d$), and Σ_1 will *inhibit* Σ_2 using $\hat{e}_1$ in a head-to-tail activator-inhibitor interaction. Ultimately, it is desired to reduce the tracking error $e_1 = p_d - x_1$ by re-adjusting p_d such that $\boldsymbol{x}$ meets the motion requirements.

Let $\hat{p}_d$ be given as

$$\hat{p}_d(t) \equiv \hat{q}_1 = q_1(t) - \hat{e}_1(t) \tag{7}$$

with other modified kinematical quantities given as

$$\hat{q}_i = q_i(t) - \hat{e}_i(t),\ i = 2, \cdots, n \tag{8}$$

therefore, in the frequency domain and using Laplace operator (s) with zero initial conditions, (6) is given as

$$\begin{aligned} \hat{e}_1 &= \frac{(\beta_0\,s^{n+1} + \beta_1\,s^n + \beta_2\,s^{n-1} + \cdots + \beta_{n+1})\,(x_1 - \hat{q}_1)}{(1+\beta_0)\,s^{n+1} + \beta_1\,s^n + \beta_2\,s^{n-1} + \cdots + \beta_{n+1}} \\ &= G_e(s)\,(x_1 - \hat{q}_1) \end{aligned} \tag{9}$$

Using (7) in (9), yields

$$x_1 = q_1 + \left\{ \frac{1 - G_e(s)}{G_e(s)} \right\} \hat{e}_1 \tag{10}$$

Consequently, the constants $\beta_i > 0$ should be chosen such that (6) is stable, and $||G_e(j\,\omega)||_\infty$ is *ideally* close to unity $\forall\omega$ in the frequency domain of interest. Doing so results in $x_1 = q_1$ as required. Interestingly, when β_i in (6) is taken as $\beta_i = \gamma_i/\epsilon^{(i)}$ with $1 \gg \epsilon > 0, \gamma_i > 0 \in \mathbb{R}$ and $\epsilon^{(i)}$ denotes ϵ to the i^{th} power, then the link with high-gain observers [20] is established where an estimate of the tracking error $e_1 = p_d - p_a$ under open-loop configuration can be used to adjust the desired input as given by (7) under activator-inhibitor configuration.

2) Stability of the activator-inhibitor system: According to lemma 4.7 in [21] and recalling Assumption 2.1, since Σ_1 is input-to-state stable, and the origin of Σ_2, i.e., (6), is globally uniformly asymptotically stable, then the origin of the cascaded system Σ_1 and Σ_2 is globally uniformly asymptotically stable.

B. Near-Optimal trajectory generator

Recalling Fig. 1a, to utilize the available information about Σ_1, and instead of using (5) with input shaping techniques for example, let the desired trajectories $\boldsymbol{q}(t)$ be the output of the *singularly perturbed* version of the trajectory generator system Σ_2 given as [17]

$$\Sigma_2 := \begin{cases} \epsilon\,\dot{\boldsymbol{\zeta}}(\tilde{t}) = \boldsymbol{A}_T\,\boldsymbol{\zeta}(\tilde{t}) + \boldsymbol{B}_T\,\tilde{\boldsymbol{u}}(\tilde{t}) \\ \boldsymbol{q}(\tilde{t}) = \boldsymbol{C}_T\,\boldsymbol{\zeta}(\tilde{t}) \end{cases} \tag{11}$$

where $\epsilon \to 0 \in \mathbb{R}$, and $\tilde{t}$ is a scaled version of the time t used in (3). Using (11), the herein proposed approach can be generalized to other systems where the matrix $\boldsymbol{A}_T$ needs to reflect the available information about Σ_1. More details about (11) can be found in [17].

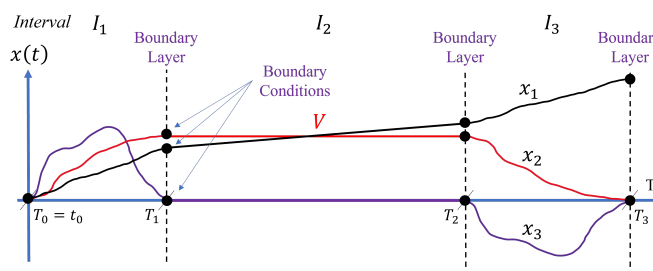

Fig. 2: An example of possible states evolution of position x_1, velocity x_2, and acceleration x_3 within three intervals, where design requirements are imposed at the boundary layers.

According to Fig. 2, a typical desired motion trajectory comprises three main intervals, i.e. acceleration, constant speed, and deceleration intervals. These trajectories capture the evolution of (11) associated with the dynamical trajectory generation system Σ_2, which makes them stand out from other reference trajectories usually obtained using signal processing techniques, c.f. [3], [10], [14], [22], [23].

When $\epsilon \to 0$ then, the trajectory becomes closer to being optimal, which clearly requires T getting larger. However, in time-critical applications, nonproductive motion [14] usually associated with acceleration and deceleration phases of motion has to be minimized to increase the application throughput. This trade-off between trajectories optimality and application throughput with enhanced tracking performance is suitably handled using optimization [14]. As discussed in [17], and $\forall t \in [T_{i-1}, T_i]$, we have [24]

$$\tilde{t} = \frac{t - T_{i-1}}{T_i - T_{i-1}},\ \ \epsilon_i = \frac{1}{T_i - T_{i-1}} \tag{12}$$

Using $\tilde{t} \in [0, 1]$ instead of $t \in [T_{i-1}, T_i]$, the index function associated with (11) is given as

$$\mathcal{J}_1^{\{i\}}(\tilde{t}) = \frac{1}{2\epsilon_i} \int_0^1 \left\{ \boldsymbol{\zeta}^{\mathrm{T}}(\tilde{t})\, \boldsymbol{Q}_i\, \boldsymbol{\zeta}(\tilde{t}) + \tilde{\boldsymbol{u}}^{\mathrm{T}}(\tilde{t})\, \boldsymbol{R}_i\, \tilde{\boldsymbol{u}}(\tilde{t}) \right\} d\tilde{t} \tag{13}$$

where the needed assumption given as in [16]. The *boundary value problem* associated with (13) is given as

$$\epsilon_i \begin{bmatrix} \dot{\boldsymbol{\zeta}}(\tilde{t}) \\ \dot{\boldsymbol{\lambda}}(\tilde{t}) \end{bmatrix} = \begin{bmatrix} \boldsymbol{A}_T & -\boldsymbol{S} \\ -\boldsymbol{Q}_i & -\boldsymbol{A}_T^{\mathrm{T}} \end{bmatrix} \begin{bmatrix} \boldsymbol{\zeta}(\tilde{t}) \\ \boldsymbol{\lambda}(\tilde{t}) \end{bmatrix} \tag{14}$$

where $\boldsymbol{S} = \boldsymbol{B}_T \boldsymbol{R}_i^{-1} \boldsymbol{B}_T^{\mathrm{T}}$, and $\boldsymbol{\lambda}(\tilde{t})$ denotes the available co-states. According to [17], the *near* optimal solution of the trajectory generator (11) $\forall \tilde{t} \in [0,1]$ is given as

$$\boldsymbol{\zeta}(\tilde{t}) = e^{(\boldsymbol{A}_T - \boldsymbol{S}\,\boldsymbol{P})\,\tilde{t}/\epsilon_i}\, \boldsymbol{l}_0^{\{i\}} + e^{(\boldsymbol{A}_T - \boldsymbol{S}\,\boldsymbol{N})\,(\tilde{t}-1)/\epsilon_i}\, \boldsymbol{r}_1^{\{i\}} \tag{15}$$

with $\boldsymbol{P} \geq 0$ and $\boldsymbol{N} \leq 0$ with $\boldsymbol{P} - \boldsymbol{N} > 0$ as the roots of the algebraic Riccati equation [16] given as

$$\begin{aligned} \mathbf{0} &= \boldsymbol{A}_T^{\mathrm{T}}\, \boldsymbol{P} + \boldsymbol{P}\, \boldsymbol{A}_T - \boldsymbol{P}\, \boldsymbol{B}_T\, \boldsymbol{R}_i^{-1}\, \boldsymbol{B}_T^{\mathrm{T}}\, \boldsymbol{P} + \boldsymbol{Q}_i \\ \mathbf{0} &= -\boldsymbol{A}_T^{\mathrm{T}}\, \boldsymbol{N} - \boldsymbol{N}\, \boldsymbol{A}_T - \boldsymbol{N}\, \boldsymbol{B}_T\, \boldsymbol{R}_i^{-1}\, \boldsymbol{B}_T^{\mathrm{T}}\, \boldsymbol{N} + \boldsymbol{Q}_i \end{aligned} \tag{16}$$

which can be solved numerically using suitable algorithms like Schur decomposition, c.f. [25].

Knowing $\boldsymbol{\zeta}(0)$ and $\boldsymbol{\zeta}(1)$ in the i^{th} interval based on the given design requirements, the needed values of $\boldsymbol{l}_0^{\{i\}}$ and $\boldsymbol{r}_1^{\{i\}}$ in (15) are given as

$$\begin{bmatrix} \boldsymbol{l}_0^{\{i\}} \\ \boldsymbol{r}_1^{\{i\}} \end{bmatrix} = \begin{bmatrix} \boldsymbol{I} & e^{-(\boldsymbol{A}_T - \boldsymbol{S}\,\boldsymbol{N})/\epsilon_i} \\ e^{(\boldsymbol{A}_T - \boldsymbol{S}\,\boldsymbol{P})/\epsilon_i} & \boldsymbol{I} \end{bmatrix}^{-1} \begin{bmatrix} \boldsymbol{\zeta}(0) \\ \boldsymbol{\zeta}(1) \end{bmatrix} \tag{17}$$

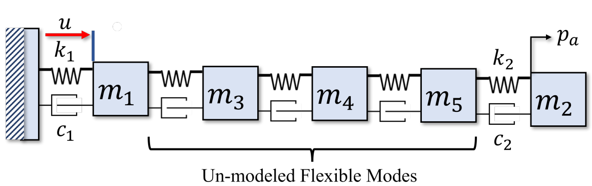

Fig. 3: A multi-mass-spring-damper model of Σ_G.

III. Simulation

Recalling Σ_G depicted in Fig. 3 which corresponds to one known rigid body mode and one known flexible mode. According to (1), Its *known* dynamics model- with $n_G = 4$- is given as [8]

$$\Sigma_G := \frac{p_a(s)}{u(s)} = \frac{c_2\, s + k_2}{a_4\, s^4 + a_3\, s^3 + a_2\, s^2 + a_1\, s + a_0} \tag{18}$$

where $a_4 = m_1 m_2, a_3 = (m_1 + m_2)c_2 + m_2 c_1, a_2 = (m_1 + m_2)k_2 + m_2 k_1 + c_2 c_1, a_1 = (k_1 + k_2)c_1$ and $a_0 = k_1 k_2$. Other un-modeled flexible modes are given in Table I.

Also, let Σ_c shown in Fig. 1a be a proportional-integral-derivative (PID) controller given as

TABLE I: The coefficients of the simulated un-modeled and supposedly unknown flexible modes according to (1).

i	$\bar{\alpha}_i/m_t$	$\bar{\zeta}_i$	$\bar{\omega}_i$
3	0.00019	0.05	49.00105
4	$5e \times 10^{-5}$	0.04973	82.88705
5	$5e \times 10^{-5}$	0.00494	340.12382

TABLE II: Σ_G The desired motion requirements are defined at the boundary layers of the motion profile [17].

States	Time Intervals					
	Interval 1		Interval 2		Interval 3	
	$\boldsymbol{x}_{G_0}^{\{1\}}$	$\boldsymbol{x}_{G_T}^{\{1\}}$	$\boldsymbol{x}_{G_0}^{\{1\}}$	$\boldsymbol{x}_{G_T}^{\{1\}}$	$\boldsymbol{x}_{G_0}^{\{1\}}$	$\boldsymbol{x}_{G_T}^{\{1\}}$
x_{G_1}	0	0.0152		0.0697		0.0849
x_{G_2}	0	0.25		0.25		0
x_{G_3}	0	0		0		0
x_{G_4}	0	0		0		0

$$\Sigma_C := k_p + k_i \frac{1}{s} + k_d \frac{s}{\tau_c\, s + 1} \tag{19}$$

with k_p, k_i and k_d as the proportional, the integral, and the derivative gains, respectively, and τ_c as the derivative-term filter time constant. Moreover, let Σ_F shown in Fig. 1a be given as a series connection consisting of Σ_G inverse, and the filter given as

$$F(s) = \left(\frac{1}{\tau_f\, s + 1} \right)^{n_f} \tag{20}$$

where $\tau_f > 0 \in \mathbb{R}$, and $n_f \geq 3 \in \mathbb{Z}$ is chosen to make Σ_F at least proper. According to [8], the following values are used $n_f = 3$, $m_1 = 42.5\,\mathrm{kg}, m_2 = 8\,\mathrm{kg}, k_1 = 10\,\mathrm{N/m}, k_2 = 7\,\mathrm{N/m}, c_1 = 10\,\mathrm{N\,s/m}, c_2 = 80\,\mathrm{N\,s/m}$, and $k_p = 468, k_i = 3.92 \times 10^5, k_d = 1.4 \times 10^5, \tau_c = 1 \times 10^{-4}$ and $\tau_f = 7.18 \times 10^{-5}$. More details about Σ_1 depicted in Fig. 1 can be found in [8].

Consider the main motion requirements specified in Table II where at the end of interval 1, a displacement of $0.0152\,\mathrm{m}$ is to be achieved, a constant velocity of $V = 0.25\,\mathrm{m/s}$ is to be maintained for a time interval of $D = T_2 - T_1 = 0.218\,\mathrm{s}$, which requires zero higher order time derivatives. Moreover, we have $T_0 = t_0 = 0$, $T = T_1 - T_0 = 0.1218\,\mathrm{s}$. With no kinematical constraints imposed, (13) is solved for each interval with uniform values of $\boldsymbol{Q}_i = 10^4\,\mathrm{diag}([1,1,10,10])$, and $\boldsymbol{R}_i = 10, i = 1,2,3$ that are *manually* tuned. Therefore, Σ_2 that generates a sub-optimal two-boundary (TB) motion profile is obtained.

Recalling (5) and Fig. 1a, consider the desired jerk signal, i.e., $l = 3$, $p_d^{(3)} := q_4$ given as

$$q_4 = \begin{cases} \gamma\, \sin^2(\omega\, t), & 0 \le t \le \frac{1}{2}T \\ -\gamma\, \sin^2(\omega\,(t-\frac{1}{2}T)), & \frac{1}{2}T \le t \le T \\ 0, & T \le t \le T+D \\ -\gamma\, \sin^2(\omega\,(t-T-D)), & T+D \le t \le \frac{3}{2}T+D \\ \gamma\, \sin^2(\omega\,(t-\frac{3}{2}T-D)), & \frac{3}{2}T+D \le t \le 2T+D \end{cases} \tag{21}$$

where the desired motion requirements given in Table II are satisfied under (21) using $\gamma = 134.8141$. Therefore, another variant of Σ_2 that generates a Sine-Squared (SS)- also known as harmonic jerk model [13]- motion profile is obtained.

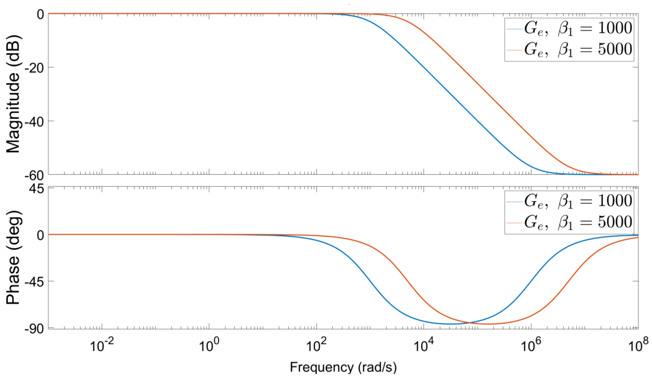

Fig. 4: The Bode plot of G_e in (22) using $\beta_1 \in \{1000, 5000\}$.

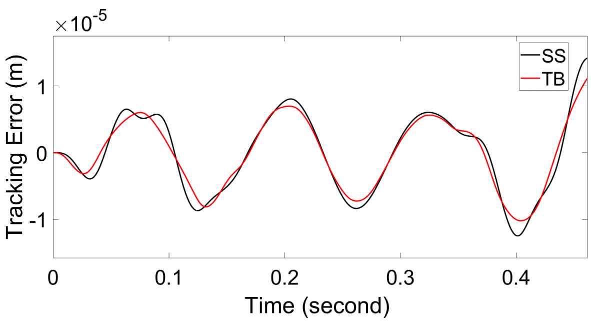

Fig. 5: The tracking error of Σ_1 under the open-loop configuration using the SS, and the TB motion profiles in Σ_2, with no external disturbance, i.e., $d = 0$.

Interestingly, despite the fact that both studied trajectories satisfy the desired motion requirements, and during their making, the SS profile given by (21) is totally unaware of the driven motion system dynamics, while the TB profile given by (15) gives voice to the known driven system dynamics. In real-time and under the open-loop configuration depicted in Fig. 1a, both trajectories are unaware of any deviation of the driven system taking place as a result of un-modeled Σ_G dynamics, or due to disturbances. To the contrary, under the activator-inhibitor configuration depicted in Fig. 1b, both trajectories get modified to adopt for these deviations. Taking $n = 2 \le \min(4,3)$, i.e., using the acceleration measurements, yields

$$\hat{e}_1 = \frac{(\beta_0\, s^3 + \beta_1\, s^2 + \beta_2\, s + \beta_3)\,(x_1 - \hat{q}_1)}{(1+\beta_0)\, s^3 + \beta_1\, s^2 + \beta_2\, s + \beta_3} \tag{22}$$

where $\beta_0 = 0.001, \beta_1 \in \{1000, 5000\}, \beta_2 = 1$, and $\beta_3 = 0.2$ are *manually* obtained such that the tracking error is minimized by including extending the frequency range of interest to include the supposedly un-modeled and unknown flexible modes. Under the herein proposed approach, dedicated algorithms utilizing the acceleration measurements [8], will be investigated separately. The Bode plots of (22) are depicted in Fig. 4.

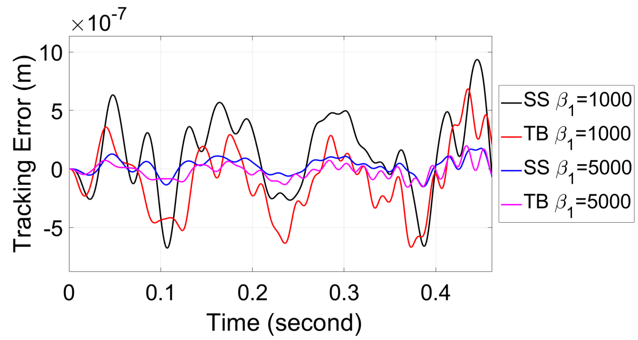

Fig. 6: The tracking error of Σ_1 under the activator-inhibitor configuration using the SS, and the TB motion profiles in Σ_2, with no external disturbance, i.e., $d = 0$, and $\beta_0 = 0.001, \beta_2 = 1, \beta_3 = 0.2, \beta_1 \in \{1000, 5000\}$.

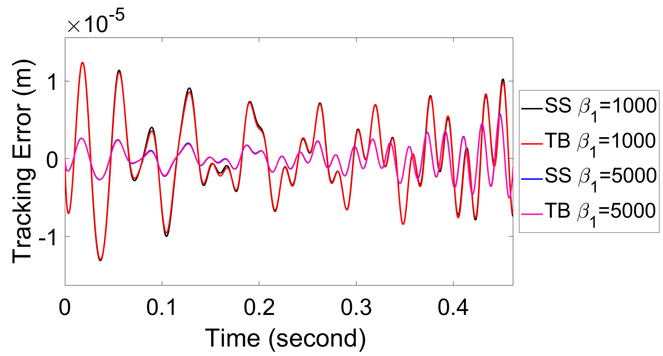

Fig. 7: The tracking error of Σ_1 under the activator-inhibitor configuration using the SS, and the TB motion profiles in Σ_2, with $\beta_0 = 0.001, \beta_2 = 1, \beta_3 = 0.2, \beta_1 \in \{1000, 5000\}$, and $d = 0.0001\, \sin(100\, t)$.

Utilizing the motion requirements given in Table II and with $d = 0$, the tracking error $e = q_1 - x_1$ under SS and TB motion profiles utilizing the open-loop configuration- see Fig. 1a- is depicted in Fig. 5, while the tracking error utilizing the head-to-tail configuration- see Fig. 1b- is depicted in Fig. 6. Comparing these results, it is clear that the tracking performance is enhanced under the head-to-tail configuration, especially when the available information of the Σ_G dynamics is utilized in creating the TB motion profile. Moreover, Fig. 6 shows that the tracking performance enhances as β_1 is increased while fixing the other coefficients of G_e. This can be justified by the increased bandwidth of G_e, i.e., the observer (6), that is depicted in Fig. 4 such that the frequencies of the flexible modes are included in the frequency of interest, and their effects can be captured by both (7) and (8).

To test the effect of disturbances on the tracking performance specifically under activator-inhibitor configuration, consider the disturbance $d = 0.0001 \sin(100\,t)$ acting on Σ_1 as shown in Fig. 1. As expected, this configuration still exhibits outstanding performance- compared to the performance of the open-loop configuration (not shown)-, especially when the former utilizes $\beta_1 = 5000$, and therefore complements the role played by Σ_C in rejecting disturbances. The results are depicted in Fig. 7.

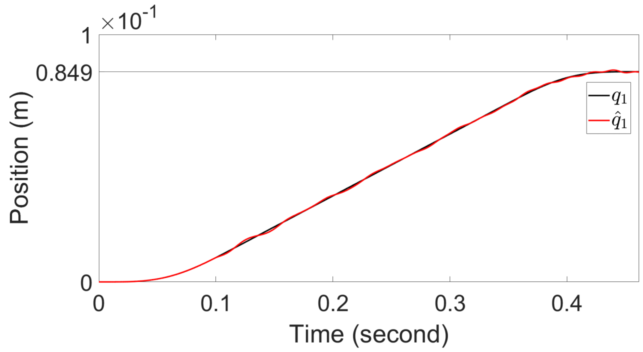

(a)

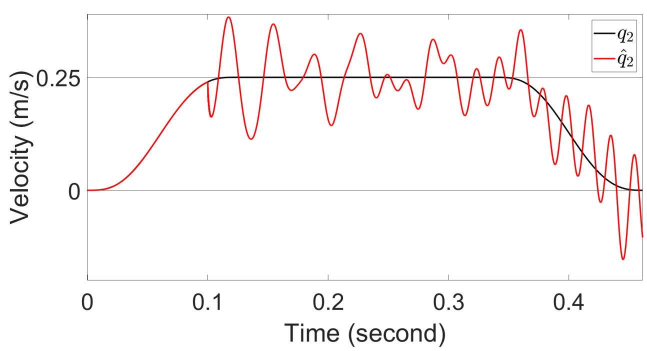

(b)

Fig. 8: The (a) position, and the (b) velocity states of Σ_2 under the activator-inhibitor configuration using the TB motion profiles with $\beta_0 = 0.001, \beta_2 = 1, \beta_3 = 0.2, \beta_1 = 5000$, and $d = 0.0001 \sin(100\,(t-0.1)), t \geq 0.1$, obtained using (7) and (8), when $n = 2$ is used.

The activator-inhibitor configuration enhances the tracking performance by utilizing (7) and (8) to modify the desired motion profile such that the effects of observed disturbances, and un-modeled dynamics are considered. Such observations can be obtained through sensory feedback measurements, or state estimators, in general. To establish this, consider the disturbance $d = 0.0001 \sin(100\,(t-0.1)), t \geq 0.1$ acting on Σ_1 under the activator-inhibitor configuration utilizing the TB motion profile. The modified profiles $\hat{q}_1$ and $\hat{q}_2$ are depicted in Fig. 8, where the modifications of q_1 and q_2 are clear after $t \geq 0.1\,\mathrm{s}$. The associated kinematics of the

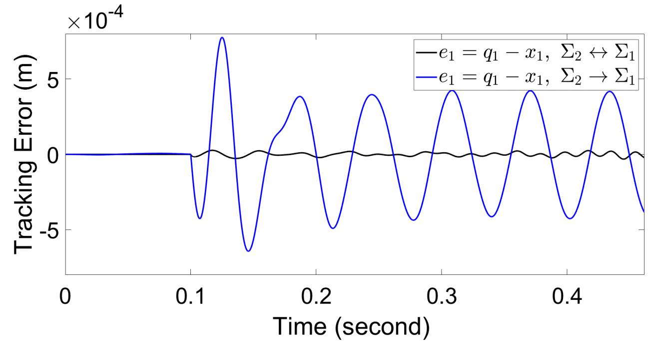

(a)

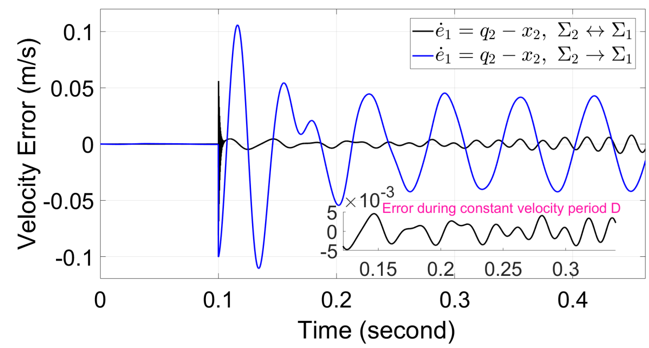

(b)

Fig. 9: The (a) position, and the (b) velocity tracking errors of Σ_1 under the open-loop configuration, and the activator-inhibitor configuration using the TB motion profiles with $\beta_0 = 0.001, \beta_2 = 1, \beta_3 = 0.2, \beta_1 = 5000$, and $d = 0.0001 \sin(100\,(t-0.1)), t \geq 0.1$, obtained using (7) and (8), when $n = 2$ is used.

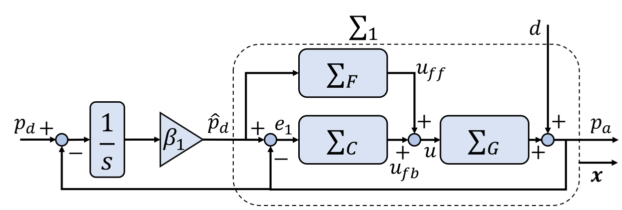

Fig. 10: Block diagram showing the LQI-like controller used.

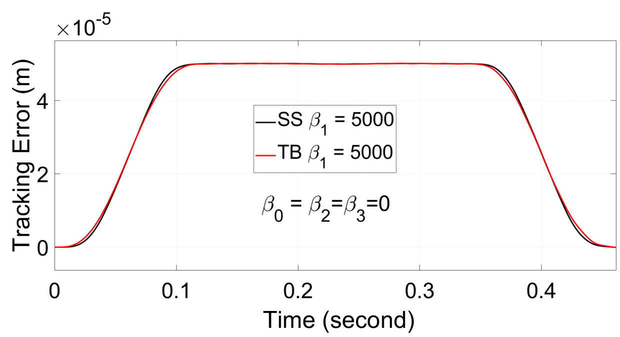

Fig. 11: The tracking error of Σ_1 under SS and TB motion profiles when the LQI-like controller is used with $d = 0$.

tracking error, i.e., $e, \dot{e}$, are depicted in Fig. 9, where in Fig. 9b the constant velocity deviation during the period D is minimum and given as $0.25 \pm 0.005\,\mathrm{m/s}$, which is crucial to many applications including wafer scanners [1], [2].

Recalling the enhanced tracking performance of the SS, and the TB motion profiles under the proposed activator-inhibitor configuration shown for example in Fig. 6, it is maybe tempting to consider its effect in isolation, i.e., by having $\beta_0 = \beta_2 = \beta_3 = 0$. This will result in a linear-quadratic-integral (LQI) like the configuration shown in Fig. 10. Using $\beta_1 = 5000$, the tracking error under the LQI-like configuration with $d = 0$ is depicted in Fig. 11. Comparing it with the tracking performance of the activator-inhibitor configuration shown in Fig. 6 reveals the latter's superiority at least for the given set of $\beta_i, i = 0, 1, 2, 3$.

IV. Conclusion

The partially known dynamics of the driven motion system were used to design near-optimal motion trajectories in the time domain using a given set of desired motion requirements. These requirements are specified at the boundaries of well-identified intervals of the motion profile. The tracking performances under the proposed cascaded activator-inhibitor configuration and a typical open-loop configuration were investigated, where the performances of the resulting near-optimal motion profile were compared to the performance under the Sine-Squared- also known as harmonic jerk model- motion profile. In the frequency domain, the activator-inhibitor configuration was realized as a transfer function whose coefficients were manually chosen to extend its bandwidth such that the distorting effects of un-modeled flexible modes, and active disturbances can be minimized while keeping the original control loops intact. Also, the link with linear quadratic regulators was highlighted.

Currently, we are developing a robust version of the proposed technique to handle existing system uncertainties and position-dependent behavior, and considering the adaptation of an input-output perspective to equip the method with data-driven machine-learning capabilities. Moreover, the use of state estimators to facilitate increasing the order of G_e, the comparison with specifically adaptive high-gain controllers, along with hardware implementation issues, and the proper choice of G_e coefficients will be handled in future work.

V. ACKNOWLEDGEMENT

The authors acknowledge the financial support of the Natural Sciences and Engineering Research Council of Canada (NSERC), the European structural and investment funds, the Czech Ministry of Education, Youth and Sports through the Operational Programme Research, Development and Education, Project MS2014+: Mobility ČVUT - VTA, Project No. CZ.02.2.69/0.0/0.0/18_053/0016980.

References

[1] M. Heertjes, B. Van der Velden, and T. Oomen, "Constrained iterative feedback tuning for robust control of a wafer stage system," *IEEE Transactions on Control Systems technology*, vol. 24, pp. 56–66, 2015.

[2] M. Heertjes, H. Butler, N. Dirkx, S. van der Meulen, R. Ahlawat, K. O'Brien, J. Simonelli, K. Teng, and Y. Zhao, "Control of wafer scanners: Methods and developments," in *American Control Conference (ACC)*, 2020, pp. 3686–3703.

[3] P. Lambrechts, M. Boerlage, and M. Steinbuch, "Trajectory planning and feedforward design for electromechanical motion systems," *Control Engineering Practice*, vol. 13, pp. 145–157, 2005.

[4] T. Vyhlídal and M. Hromčík, "Parameterization of input shapers with delays of various distribution," *Automatica*, vol. 59, pp. 256–263, 2015.

[5] L. Dai, X. Li, Y. Zhu, M. Zhang, and C. Hu, "The generation mechanism of tracking error during acceleration or deceleration phase in ultraprecision motion systems," *IEEE Transactions on Industrial Electronics*, vol. 66, pp. 7109–7119, 2018.

[6] K. Verkerk, H. Butler, and P. van den Bosch, "Improved disturbance rejection for high precision systems through estimation of the flexible modes," in *Proceedings of the IEEE Conference on Control Applications*, 2015, pp. 1191–1196.

[7] A. Dumanli and B. Sencer, "Robust trajectory generation for multiaxis vibration avoidance," *IEEE/ASME Transactions on Mechatronics*, vol. 25, pp. 2938–2949, 2020.

[8] Y. Al-Rawashdeh, M. Al Janaideh, and M. Heertjes, "A suppress-excite approach for online trajectory generation of uncertain motion systems," *Mechanical Systems and Signal Processing*, vol. 186, p. 109769, 2023.

[9] K. Erkorkmaz, S. E. Layegh, I. Lazoglu, and H. Erdim, "Feedrate optimization for freeform milling considering constraints from the feed drive system and process mechanics," *CIRP Annals*, vol. 62, pp. 395–398, 2013.

[10] B. Sencer and S. Tajima, "Frequency optimal feed motion planning in computer numerical controlled machine tools for vibration avoidance," *Journal of Manufacturing Science and Engineering*, vol. 139, 2017.

[11] Y. Kasemsinsup, M. Heertjes, H. Butler, and S. Weiland, "Exact plant inversion of flexible motion systems with a time-varying state-to-output map," in *Proceedings of the European Control Conference*, 2016, pp. 2483–2488.

[12] J. Dewey, K. Leang, and S. Devasia, "Experimental and theoretical results in output-trajectory redesign for flexible structures," in *Proceesings of 35th IEEE Conference on Decision and Control*, 1998, pp. 4210–4215.

[13] Y. Fang, J. Hu, W. Liu, Q. Shao, J. Qi, and Y. Peng, "Smooth and time-optimal s-curve trajectory planning for automated robots and machines," *Mechanism and Machine Theory*, vol. 137, pp. 127–153, 2019.

[14] Y. Al-Rawashdeh, M. Al Janaideh, and M. Heertjes, "Kinodynamic generation of wafer scanners trajectories used in semiconductor manufacturing," *IEEE Transactions on Automation Science and Engineering*, 2022.

[15] H. Yavuz, S. Mıstıkoğlu, and S. Kapucu, "Hybrid input shaping to suppress residual vibration of flexible systems," *Journal of Vibration and Control*, vol. 18, pp. 132–140, 2012.

[16] P. Kokotović, H. Khalil, and J. O'reilly, *Singular perturbation methods in control: analysis and design*. SIAM, 1999.

[17] Y. Al-Rawashdeh, V. Reddy, M. Al Saaideh, A. Boker, H. Eldardiry, and M. Al Janaideh, "Near-optimal trajectory generation for flexible motion systems using two-boundary approach," in *2023 European Control Conference (ECC)*, 2023, pp. 1–6.

[18] P. Fife, "On modelling pattern formation by activator-inhibitor systems," *Journal of Mathematical Biology*, vol. 4, no. 4, pp. 353–362, 1977.

[19] A. Turing, "The chemical basis of morphogenesis," *Bulletin of mathematical biology*, vol. 52, no. 1-2, pp. 153–197, 1990.

[20] H. Khalil, "High-gain observers in nonlinear feedback control," in *2008 International Conference on Control, Automation and Systems*, 2008, pp. xlvii–lvii.

[21] ——, *Nonlinear systems*, 3rd ed. Prentice Hall, 2002.

[22] K. Chen and R. Fung, "The point-to-point multi-region energy-saving trajectory planning for a mechatronic elevator system," *Applied Mathematical Modelling*, vol. 40, no. 21-22, pp. 9269–9285, 2016.

[23] H. Seki and S. Tadakuma, "Minimum jerk control of power assisting robot on human arm behavior characteristic," in *Proceedings of the IEEE International Conference on Systems, Man and Cybernetics*, 2004, pp. 722–727.

[24] L. Biagiotti and C. Melchiorri, *Trajectory planning for automatic machines and robots*. Springer Science & Business Media, 2008.

[25] C. Paige and C. Van Loan, "A schur decomposition for hamiltonian matrices," *Linear Algebra and its applications*, vol. 41, pp. 11–32, 1981.